Model dependence of the pion form factor extracted from pion electroproduction

Robert J. Perry,* Ayşe Kızılersü, and Anthony W. Thomas
CSSM and ARC Centre of Excellence for Particle Physics at the Tera-scale, Department of Physics, University of Adelaide, Adelaide SA 5005, Australia

(Received 6 February 2019; revised manuscript received 20 May 2019; published 20 August 2019)

In 2008 the Jefferson Laboratory F_π Collaboration released results for the pion electromagnetic form factor, which they extracted from pion electroproduction data. The measured values for the pion form factor are model dependent, and require the use of the Vanderhaeghen, Guidal, and Laget Regge model for their extraction. While agreement between this model and data is impressive, the theoretical implementation of gauge invariance is less satisfying. We would like to establish how well the extracted form factor corresponds to the true form factor. To do this, we use a simple toy model, which imposes gauge invariance in a more theoretically satisfying way. The model form factor is extracted from our model cross section using the method employed by the F_π Collaboration to extract the experimental pion form factor. We conclude that the reconstructed model form factor is a reasonable representation of the true model form factor for the kinematics chosen, although we note that the extracted form factor is smaller than the true form factor. This suggests that current extracted values of the pion form factor may be overestimated.

DOI: 10.1103/PhysRevC.100.025206

I. INTRODUCTION

The pion is the pseudo-Goldstone boson associated with the dynamical breaking of the approximate chiral symmetry of quantum chromodynamics (QCD). Because of its characteristically light mass, the pion yields the longest range contribution to low energy hadronic observables. This dominance at low energies means both that the pion is the most easily studied meson and also that a deep understanding of the pion is necessary to investigate the low energy, nonperturbative behavior of QCD.

One clear window into the complicated behavior of the pion is its electromagnetic form factor $F_\pi(Q^2)$. This Lorentz invariant structure function encodes the nonperturbative behavior of the electromagnetically charged partons inside the pion and may be related to the the pion's transverse charge distribution [1]. Many different complementary theoretical descriptions exist of the pion form factor. At low photon virtuality, the pion form factor may be calculated from first principles using lattice QCD but as the photon virtuality increases the extraction of the pion form factor becomes more difficult. Novel techniques have allowed extraction of the pion form factor out to about $6\,\mathrm{GeV}^2$ [2]. Models based on QCD may be extended to higher momenta. For example, the pion electromagnetic form factor was reasonably well predicted in the NJL model [3]. More complicated models, based on the Dyson-Schwinger approach are also able to predict to good accuracy the current experimental data [4].

Finally, in the very large momentum limit, the result of Lepage and Brodsky [5] is expected to hold:

$$Q^2 F_\pi(Q^2) \to 16\pi f_\pi^2 \alpha_s(Q^2), \tag{1}$$

where $f_\pi \approx 0.132\,\mathrm{GeV}$ is the pion decay constant, and $\alpha_S(Q^2)$ is the strong coupling constant. More modern analyses [6] have shown that this relation is applicable at lower energy scales, if one correctly takes into account the effects of the pion's valence quark parton distribution amplitude, rather than using an asymptotic form correct in the limit of infinite momentum. Because this result is derived in the context of perturbative QCD, probing the high momentum behavior of F_π gives information on the transition from the nonperturbative regime to the perturbative regime in QCD. Agreement with this relation would give confidence that the asymptotic limit of QCD is understood. As is shown below in Fig. 1, the current data indicates that we have not yet probed high enough energies for the above relation to hold.

The pion form factor is also an experimentally difficult observable to measure at larger momenta. At low photon virtuality, the pion form factor may be measured directly from elastic $e^- + \pi^+$ scattering. However, because of kinematic limitations of the pion beam, this approach only allows an extraction of the pion form factor up to approximately $0.3\,\mathrm{GeV}^2$ [7]. Thus for larger momentum transfer values, another technique must be used. We call this region between the failure of direct measurement in $e^- + \pi^+$ scattering and the onset of perturbative QCD the *intermediate* momentum region (see Fig. 1). Modern extractions of the pion electromagnetic form factor in this intermediate region utilize pion electroproduction.

In pion electroproduction, information about the pion form factor is obtained by scattering an electron off the pion cloud of the nucleon. There are a number of complications to this approach which must be addressed to extract the pion form factor from this process.

First, there is an interference between the t-channel term, which contains the pion form factor, and the s- and u-channel

*robert.perry@adelaide.edu.au

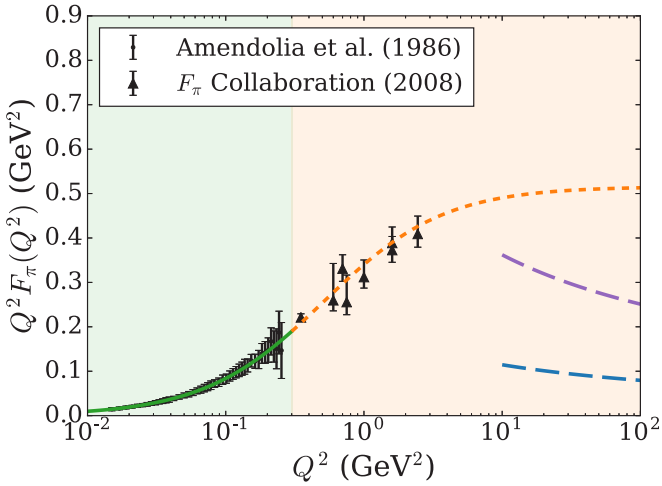

FIG. 1. Experimental data for the pion electromagnetic form factor. Low energy data (small black circles in low energy region) is taken from Ref. [7], and intermediate energy data (large black triangles) is taken from Ref. [8]. Note that the intermediate momentum region is defined to be the region between the failure of direct measurement of $e^-\pi^+$ elastic scattering and the scale at which perturbative QCD becomes applicable. For comparison, the two different asymptotic limits of the electromagnetic form factor are also shown (long dashed lines). The bottom curve is the result of assuming the asymptotic form of the pion light cone distribution function, while the middle curve is the result of a more modern analysis (see Ref. [6]). The energy scale at which this result becomes applicable is still an open question. The top curve (short dashed line) is the monopole parametrization of the data.

terms, which contain the nucleon form factors. Thus any extraction of the pion form factor from this process must understand how these interference terms effect the overall measured cross section.

Secondly, the pion is initially off-shell. The pion's virtuality is measured by the t Mandelstam variable. Importantly, because of the kinematics of pion electroproduction, t is kinematically constrained to be negative, whereas the on-shell pion form factor should be obtained by probing an on-shell pion, that is, at $t = m_\pi^2 > 0$. Thus, while it is clear that pion electroproduction should be able to give us information about the pion form factor, it is not immediately obvious how closely related the off-shell pion is to the on-shell pion measured in direct $e^- + \pi^+$ scattering. Previously, this question was addressed in the context of a Bethe-Salpeter approach [9]. There, the authors found that the "pion form factor" increased in magnitude as the pion deviated further off-shell. We place pion form factor in quotes here to emphasize, as do the authors of the paper, that one may only truly talk about the pion form factor when the pion is on-shell, because there is no unique definition of an off-shell state. This result would seem to indicate that care must be taken when extracting the pion form factor to ensure that variation of the pion form factor from pion's "off-shellness" is minimized.

To extract the pion form factor from the electroproduction data, a model of the differential cross section must be used. The F_π Collaboration use the Vanderhaeghen, Guidal, and Laget (VGL) model, a Regge model in which the polelike propagators of a Born term model are replaced by Regge propagators where the single particles are replaced by the exchange of a family of particles with the same internal quantum numbers. To incorporate the extended structure of the pion in the VGL model, the pion's electromagnetic form factor is included in the matrix element, which is given by

$$i\mathcal{M}^\mu_{\rm VGL} = i\mathcal{M}^\mu_{\rm R} F_\pi(Q^2), \tag{2}$$

where $i\mathcal{M}^\mu_{\rm R}$ is the Reggized gauge invariant amplitude for the scattering of pointlike nucleons and pions, and $F_\pi(Q^2)$ is the electromagnetic form factor. A second term describes the exchange of a rho meson instead of the pion in the t channel, but it is irrelevant for the point we are trying to make, so we ignore it here. This matrix element leads to a differential cross section of the form,

$$\left(\frac{d\sigma_L}{dt}\right)_{\rm VGL} = (F_\pi(Q^2))^2 \left(\frac{d\sigma_L}{dt}\right)_{\rm R}, \tag{3}$$

where $(d\sigma_L/dt)_R$ is termed the *longitudinal* cross section, obtained from the matrix element $i\mathcal{M}^\mu_{\rm R}$. In principle, only the t-channel diagram can contribute to the form factor $F_\pi(Q^2)$, because the s- and u-channel diagrams give information about the nucleon form factors. To write the matrix element as is done above, one must approximate the pion and proton Dirac form factors to be equal. For a comparison of the relevant pion and proton form factors in the region probed by pion electroproduction, see Fig. 2.

Following the above discussion, we now wish to test whether this approximation leads to inconsistencies in the extracted pion form factor. To do this, we choose a simple toy

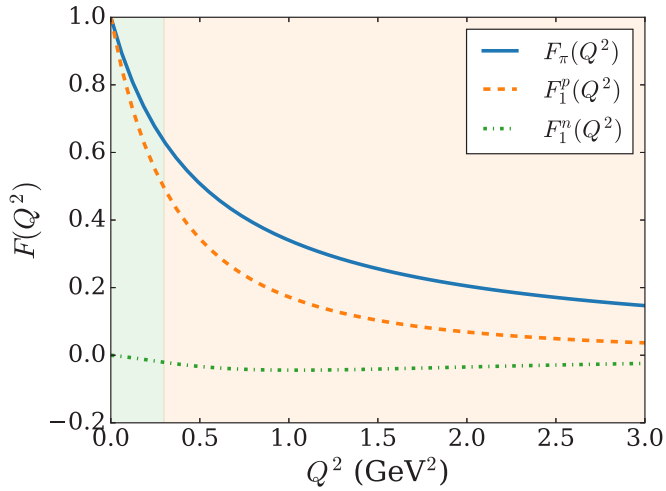

FIG. 2. Comparison of the pion electromagnetic form factor (solid blue curve) with the proton (dashed curve) and neutron (dot-dashed curve) Dirac form factors. As is conventional, we have parametrized the pion form factor with a monopole form $F_\pi(Q^2) = (1 + Q^2/\Lambda_\pi^2)^{-1}$, while we parametrize the proton Dirac form factor with a dipole form $F_1^p(Q^2) = (1 + Q^2/\Lambda_p^2)^{-2}$. For the neutron, we use the Galster parametrization [10]. The parameters Λ_π and Λ_p may be related to the electromagnetic charge radius of the respective particle. The shaded regions correspond to the same momentum regions shown in Fig. 1.

model, which allows us to calculate form factors and cross section exactly. We then use the method employed by the F_π Collaboration to attempt to extract the toy model's pion form factor from our cross section. This allows us to see how well we are able to extract the form factor using this approach. While the use of a toy model prevents us from making direct statements about the physical extracted pion form factor, we suggest that the conclusions drawn from our toy model may carry over qualitatively to the physical form factor.

II. KINEMATICS AND PRELIMINARIES

Before discussing the VGL model in more detail, we first introduce our conventions for kinematic variables and structure functions. We label external momenta as shown in Fig. 3, where overall momentum conservation gives $p+q=p'+p_\pi$. This convention for external particle momenta determines how momentum flows into the loop diagrams.

We define the Mandelstam variables,

$$s = p_s^2 = (p+q)^2 = (p'+p_\pi)^2 \equiv W^2, \tag{4}$$

$$t = p_t^2 = (p_\pi - q)^2 = (p-p')^2, \tag{5}$$

$$u = p_u^2 = (p-p_\pi)^2 = (p'-q)^2. \tag{6}$$

Finally, we define $Q^2=-q^2$ so that spacelike momenta are positive. These three momenta (Q^2, W, and t) allow one to fully describe the cross section. The measured unpolarized differential cross section may be separated according to the polarization states of the virtual photon into transverse (T), longitudinal (L) polarizations, as well as two interference terms (LT and TT) [11]:

$$(2\pi)\frac{d^2\sigma}{dt\,d\phi} = \frac{d\sigma_T}{dt} + \epsilon\frac{d\sigma_L}{dt} + \sqrt{2\epsilon(\epsilon+1)}\frac{d\sigma_{LT}}{dt}\cos\phi + \epsilon\frac{d\sigma_{TT}}{dt}\cos 2\phi, \tag{7}$$

where ϵ is a measure of the virtual photon polarization, and is related to experimental quantities via

$$\epsilon = \left(1 + \frac{2|\vec{q}|^2}{Q^2}\tan^2\frac{\theta_e}{2}\right)^{-1}, \tag{8}$$

$\vec{q}$ is the three-momentum of the virtual photon, and θ_e is the angle between the initial and final electron three-momentum. This decomposition is important because it is well known that the t-channel pion exchange diagram dominates the longitudinal differential cross section $d\sigma_L/dt$ [12]. It was shown previously that rho meson exchange is suppressed in the longitudinal cross section by approximately an order of magnitude (see Fig. 4, Ref. [13]). Thus a model which precisely predicts the longitudinal differential cross section has a good chance of extracting the pion form factor.

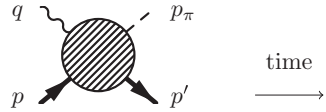

FIG. 3. Hadronic component on pion electroproduction in the one-photon exchange approximation (o.p.e.a.). Overall conservation of momentum gives $p+q=p'+p_\pi$. This sets the direction of the external momenta.

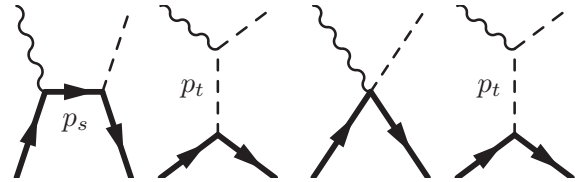

FIG. 4. Born term model for pion electroproduction. The pion form factor is measured in pion electroproduction via the t-channel diagram. The second t-channel diagram corresponds to the exchange of a virtual rho meson. There is no u channel diagram because in our effective field theory, the neutron is neutral at tree level.

III. THE VGL MODEL

Before examining the model dependence of the extracted pion form factor, we must first understand the VGL model. Originally developed by Vanderhaeghen Guidal, and Laget as a model of pion photoproduction [14], it was quickly realized that the generalization to electroproduction was straightforward, leading to the so-called VGL model [13]. The VGL model is based on the t-channel pion exchange Born diagram, shown in Fig. 4. The t-channel diagram is not gauge invariant on its own, and requires the inclusion of the s channel and Kroll-Ruderman terms to restore gauge invariance. The t-channel diagram in which a rho meson is exchanged instead of a pion is also included. This diagram is independently gauge invariant, so no accompanying diagrams must be added to preserve gauge invariance. To improve agreement between the model and data, the pion propagator is *Reggeized*, which amounts to replacing the pion and rho meson propagators $S_F^{\pi/\rho}(t)$ with its Reggeized version $S_R^{\pi/\rho}(t)$. To understand the VGL model, it helps to begin by examining the Born term model upon which it is based.

A. The Born term model

Using the Feynman rules outlined in Appendix A of Ref. [15], we can show that the Born term model (BTM) arising from this Lagrangian is given by

$$i\mathcal{M}^\mu_{\rm BTM} = i\mathcal{M}^\mu_s + i\mathcal{M}^\mu_t + i\mathcal{M}^\mu_{\rm K.R.}, \tag{9}$$

where the associated diagrams are given in Fig. 4. We have ignored the rho meson term shown above, as it is gauge invariant on its own, and adds nothing to the understanding of the VGL model. The three terms are denoted $i\mathcal{M}^\mu_s$, $i\mathcal{M}^\mu_t$, and $i\mathcal{M}^\mu_{\rm K.R.}$, respectively:

$$i\mathcal{M}^\mu_s = \frac{g_A}{\sqrt{2}f_\pi}\bar{u}_N(p',s')\gamma_5 \not{p}_\pi S_F^N(p_s) \tag{10}$$

$$\times(-ie\gamma^\mu)u_N(p,s), \tag{11}$$

$$i\mathcal{M}^\mu_t = \frac{g_A}{\sqrt{2}f_\pi}\bar{u}_N(p',s')\gamma_5 \not{p}_t u_N(p,s) S_F^\pi(p_t) \tag{12}$$

$$\times(-ie)(p_t+p_\pi)^\mu, \tag{13}$$

$$i\mathcal{M}^\mu_{\rm K.R.} = -\frac{g_A e}{\sqrt{2}f_\pi}\bar{u}_N(p',s')\gamma_5\gamma^\mu u_N(p,s). \tag{14}$$

Thus the Born term model matrix element is

$$i\mathcal{M}^{\mu}_{\mathrm{BTM}} = \frac{g_A}{\sqrt{2}f_\pi}\bar{u}_N(p',s')\gamma_5 \not{p}_\pi S_F^N(p_s)(-ie\gamma^\mu)u_N(p,s) + \frac{g_A}{\sqrt{2}f_\pi}\bar{u}_N(p',s')\gamma_5 \not{p}_t u_N(p,s) S_F^\pi(p_t)(-ie)(p_t+p_\pi)^\mu - \frac{g_A e}{\sqrt{2}f_\pi}\bar{u}_N(p',s')\gamma_5\gamma^\mu u_N(p,s). \tag{15}$$

B. Transforming the Born term model to the VGL model

One may obtain the VGL model by first Reggeizing this amplitude, and then further multiplying the amplitude by the pion form factor. Importantly, in replacing the Feynman propagators with their Regge versions, gauge invariance must be preserved. One may understand the Reggeization of the amplitude used in the VGL model as the multiplication of the Born term model amplitude by a *single momentum-dependent factor* $S_F^{\pi\,-1}(p_t)S_R^\pi(p_t)$, where $S_F^\pi(p_t)$ is the Feynman propagator, and $S_R^\pi(p_t)$ is the Reggeized pion proagator. Thus

$$i\mathcal{M}^{\mu}_{\mathrm{R}} = S_F^{\pi\,-1}(p_t)S_R^\pi(p_t)\left[i\mathcal{M}^{\mu}_{\mathrm{BTM}}\right]. \tag{16}$$

More will be said about this procedure later. In particular, we will explain why it is helpful to think of the Reggeization step as a multiplicative procedure on the amplitude. Reggeizing the amplitude in this way leads to the Reggeized matrix element $i\mathcal{M}^{\mu}_{\mathrm{R}}$:

$$i\mathcal{M}^{\mu}_{\mathrm{R}} = \frac{g_A}{\sqrt{2}f_\pi}\bar{u}_N(p',s')\gamma_5 \not{p}_\pi S_F^N(p_s)S_F^{\pi\,-1}(p_t)S_R^\pi(p_t)(-ie\gamma^\mu)u_N(p,s) + \frac{g_A}{\sqrt{2}f_\pi}\bar{u}_N(p',s')\gamma_5 \not{p}_t u_N(p,s) S_R^\pi(p_t)(-ie)(p_t+p_\pi)^\mu - \frac{g_A e}{\sqrt{2}f_\pi}\bar{u}_N(p',s')S_F^{\pi\,-1}(p_t)S_R^\pi(p_t)\gamma_5\gamma^\mu u_N(p,s). \tag{17}$$

The pion form factor is then introduced as

$$i\mathcal{M}^{\mu}_{\mathrm{VGL}} = i\mathcal{M}^{\mu}_{\mathrm{R}}F_\pi(Q^2), \tag{18}$$

where $F_\pi(Q^2)$ is the electromagnetic form factor. Having briefly discussed the VGL model, we will now explain the process by which the pion form factor is extracted from experimental data.

C. Fitting the VGL model to data

We can now summarize the procedure used by the F_π Collaboration to fit the VGL model to experimental data. The functional form of the pion form factor is taken to be the monopole form:

$$F_\pi(Q^2) = \frac{1}{1+Q^2/\Lambda_\pi^2}, \tag{19}$$

and the transition form factor for the ρ is assumed to have the same functional form:

$$F_{\gamma\rho\pi}(Q^2) = \frac{1}{1+Q^2/\Lambda_\rho^2}, \tag{20}$$

where Λ_π^2 and Λ_ρ^2 are the only free parameters in the model. As mentioned previously, the longitudinal cross section is insensitive to the rho meson, so effectively only Λ_π^2 must be fit to obtain the longitudinal cross section.

For some points it sufficed to fit the differential cross section measured fixed Q^2 and W values for small $|t|$ values by varying the value of the Λ_π^2 value. In this case, the extracted pion form factor corresponds to the best fit value of Λ_π^2. However, for a number of kinematic points, this procedure was not sufficient to extract the pion form factor well. An example of this is shown in the first plot of Fig. 5. Here, the VGL model fails to completely describe the t dependence of the data. In this case each data point was fitted to the corresponding measured differential cross section point individually. Thus for each data point, there is a corresponding extracted Λ_π^2. This is shown in the second plot of Fig. 5. Note that in general, data points measured at smaller values of t tend to result in larger values of Λ_π^2, and thus larger values of $F_\pi(Q^2)$. It was suggested that this is from interfering backgrounds not included in the VGL model [8]. In practice, an extrapolation of Λ_π^2 to the minimum experimentally allowed t value for the chosen Q^2 and W values is performed and it is this value of Λ_π^2 which is taken to correspond to the best estimate of $F_\pi(Q^2)$. These values are shown in Fig. 1.

While the agreement between the VGL model and data is quite good, as we have shown, there is room to improve the implementation of gauge invariance. We aim to understand whether it is worth improving the implementation of gauge invariance, by studying whether the current approach can successfully extract the form factor in a toy model. To do this, we must first understand the constraints placed on the amplitude by gauge invariance.

IV. GAUGE INVARIANCE AND THE WARD GREEN TAKAHASHI IDENTITIES

We are interested in extracting the pion electromagnetic form factor in the intermediate Q^2 region. In lieu of an exact solution from QCD, we can attempt to build a model for the interaction. In this case, respecting the symmetries of the fundamental theory is essential. The electromagnetic gauge symmetry is one such symmetry which is exactly respected in pion electroproduction. We can thus use this condition to constrain the form of the pion electroproduction amplitude. We begin by recalling some basic facts about electromagnetic gauge invariance.

In QED, it is well known that the gauge invariance of the interaction is expressed through relationships between

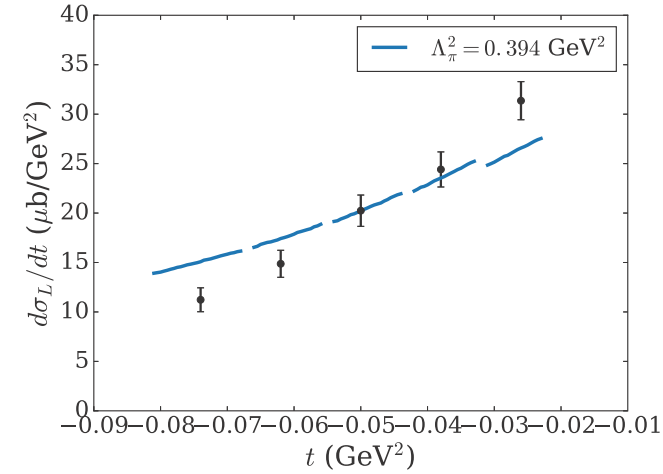

(a)

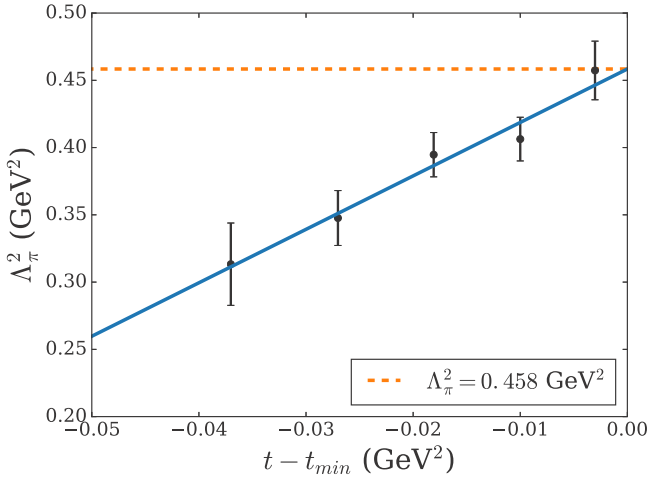

(b)

FIG. 5. Plots adapted from the F_π Collaboration's extraction of the pion form factor (Ref. [8], Fig. 2, Fig. 5). The upper plot (a) shows the fitted longitudinal cross section, compared to experimental data. Note that the theory curve for the longitudinal cross section is plotted for a single value of Λ_π^2 to demonstrate the general agreement of the VGL Model with data. As explained, when performing the extraction, the model is fit to each data point independently. The bottom plot (b) shows the corresponding extracted values of Λ_π^2. The best fit value for Λ_π^2 for this set of kinematics ($Q^2 = 0.6\,\text{GeV}^2$, $W = 1.95\,\text{GeV}$) is $\Lambda_\pi^2 = 0.458 \pm 0.031^{+0.255}_{-0.068}\,\text{GeV}^2$ [8].

the n and $n+1$ point Green's functions. These identities are collectively referred to as the *Ward Green Takahashi Identities* [16–18]. In Ref. [19] Nishijima showed that the Ward Green Takahashi Identities are satisfied for a general gauge invariant Lagrangian, independent of the explicit form. The implication of this is that in an effective field theoretic description of pion electroproduction, the Ward Green Takahashi Identities from QED must be satisfied. The generic form for these identities in momentum space is

$$q_\mu \Gamma_n^{\mu\cdots}(p, \ldots; q) = \Phi_n(\Gamma_{n-1}, \Gamma_{n-2}, \ldots, \Gamma_2), \tag{21}$$

where q_μ is an external boson momentum contracted with the appropriate Lorentz index of a Green's function. These identities equate this contraction to a combination of lower Green's functions, denoted symbolically here by Φ_n. In particular, we are interested in

$$-iq_\mu \Gamma^\mu(p, p') = S_F^{-1}(p') - S_F^{-1}(p), \tag{22}$$

and

$$-iq_\mu \Delta^\mu(q; p_\pi, p', p) = \Gamma(p_\pi - q, p', p) + \Gamma(p_\pi, p' - q, p) - \Gamma(p_\pi, p', p + q), \tag{23}$$

where Γ^μ and $S_F(p)$ are the renormalized vertices and propagators, respectively, and Δ^μ and Γ are the vector four-point and scalar three-point vertices, respectively. For a bosonic particle, the most general forms are

$$S_F(p) = \frac{i}{p^2 - m^2 - \Sigma(p^2)}, \tag{24}$$

and

$$\Gamma^\mu(p, p') = (p + p')^\mu f_1(p^2, p'^2, q^2) + (p - p')^\mu f_2(p^2, p'^2, q^2). \tag{25}$$

The equations for a fermionic particle are more complicated (the most general form of the self-energy contains two Lorentz invariant functions, and the most general vertex may be decomposed into 12 Lorentz invariant functions). In this paper, we consider a model in which all particles involved in the interaction are *bosonic*, so we make no further mention of the fermionic case.

Importantly, the Ward Green Takahashi Identities are also satisfied order-by-order in perturbation theory. In this case, the full propagators and vertices are replaced with their approximations, valid at the specific order of perturbation theory being calculated. Not only are they an important check of the model's validity, but gauge invariance is essential in ensuring renormalizability and unitarity of the theory.

V. GAUGE INVARIANCE IN THE VGL MODEL

The Ward Green Takahashi Identities are valid for arbitrary matrix elements. In the limit that the external particles are on their respective mass shells, one can show that the Ward Green Takahashi Identity for the pion electroproduction amplitude reduces to

$$q_\mu \mathcal{M}^\mu = 0. \tag{26}$$

In any gauge invariant model, this property must be upheld, to ensure that current conservation was preserved. One can show that the VGL model does indeed satisfy this requirement. Because it is central to our discussion of the appropriateness of the pion form factor in the VGL model amplitude, we will show how gauge invariance is satisfied in this model. To begin with, however, we consider the simpler case of the Born term model.

Gauge invariance in the Born term model

The Born term model is defined by the matrix element, $i\mathcal{M}^\mu_{\text{BTM}}$, which is defined by Eq. (15). We consider contracting

q_μ into this matrix element:

$$iq_\mu \mathcal{M}^\mu_{\rm BTM} = \frac{g_A e}{\sqrt{2} f_\pi} \bar{u}_N(p', s') \Big[\gamma_5 \not{p}_\pi \frac{(\not{p}_s + m_N)}{s - m_N^2} \not{q} + \gamma_5 \not{p}_t \frac{q \cdot (p_t + p_\pi)}{t - m_\pi^2} - \gamma_5 \not{q} \Big] u_N(p, s). \quad (27)$$

After some algebra, one arrives at

$$iq_\mu \mathcal{M}^\mu_{\rm BTM} = \frac{g_A e}{\sqrt{2} f_\pi} \bar{u}_N(p', s') \gamma_5 [\not{p}_\pi - \not{p}_t - \not{q}] u_N(p, s). \quad (28)$$

By noting that $p_t = p_\pi - q$, it is possible to see that the hadronic current is conserved. Note that this is true even for $q^2 \neq 0$, as it must be. Importantly though, tracing the origins of the terms back, it is possible to see that a cancellation occurs between the t, s, and Kroll-Ruderman terms. In other words, if one wishes to modify the above form of the Born term model, one must do it in such a way that the cancellation persists.

It is reasonably straightforward to show that by multiplying each of the diagrams by a different momentum-dependent function, the only possible way to ensure gauge invariance is to set all of these functions equal. In other words, if gauge invariance is preserved for the amplitude $i\mathcal{M}^\mu$, it will also be preserved for the amplitude $f \times [i\mathcal{M}^\mu]$, where f is a general momentum-dependent function. It is this result which is essential to understand the VGL model's implementation of gauge invariance, and is the reason we described the Reggeization of the amplitude as a multiplicative operation. Recalling that it is possible to write the Reggeized amplitude $i\mathcal{M}^\mu_{\rm R}$ as defined by Eq. (16), it should be clear that the Reggeized amplitude is still gauge invariant. Finally, the structure of the pion is incorporated by multiplying the Reggeized amplitude by the pion form factor $F_\pi(Q^2)$. We thus arrive at the VGL model matrix element:

$$i\mathcal{M}^\mu_{\rm VGL} = i\mathcal{M}^\mu_{\rm R} F_\pi(Q^2). \quad (29)$$

By writing the VGL model amplitude in this form, it is easy to see why gauge invariance is preserved; it is a consequence of the underlying Born term diagrams which arise from a gauge invariant Lagrangian. This completes our discussion of the VGL model. To determine whether this somewhat unnatural approximation leads to any inconsistencies in the extracted form factor, we will repeat the F_π analysis in a simple model whose form factor we can calculate exactly. This will allow us to determine how well one can reconstruct the pion form factor.

VI. A TOY MODEL OF PION ELECTROPRODUCTION

We have now seen how the VGL model preserves gauge invariance. To determine the consequences for the extracted pion form factor, we will examine how well the approach works in a simple toy model, where we can calculate the form factor and cross section exactly. Our criteria for a suitable model is twofold.

(1) It must be gauge invariant.
(2) The nucleon and pion must have different form factors.

A suitable model for this is Miller's simple model of the nucleon's electromagnetic form factors, described in Ref. [20]. In this simple model, we consider a quantum field theory describing the interaction of a scalar "nucleon" and scalar "pion." To be clear, we define a scalar "nucleon" doublet Ψ_N,

$$\Psi_N = \begin{bmatrix} \psi_p \\ \psi_n \end{bmatrix}, \quad (30)$$

and a scalar "pion" triplet $\boldsymbol{\pi}$,

$$\boldsymbol{\pi} = \begin{bmatrix} \pi^+ \\ \pi^- \\ \pi^0 \end{bmatrix}, \quad (31)$$

where $\pi^+ = (\pi_1 - i\pi_2)/\sqrt{2}$ and $\pi^- = (\pi_1 + i\pi_2)/\sqrt{2}$; we may write the Lagrangian as

$$\mathcal{L} = \tfrac{1}{2}(\partial_\mu \Psi_N)^2 - \tfrac{1}{2} m_N^2 \Psi_N^2 + \tfrac{1}{2}(\partial_\mu \boldsymbol{\pi})^2 - \tfrac{1}{2} m_\pi^2 \boldsymbol{\pi}^2 - g_{\pi N} \Psi_N^\dagger \boldsymbol{\tau} \cdot \boldsymbol{\pi} \Psi_N, \quad (32)$$

where $\boldsymbol{\tau}$ is the isospin vector. Gauging the Lagrangian leads to electromagnetic interactions between the charged particles in the theory. We are interested in (scalar) $\gamma^* + p \to \pi^+ + n$. To preserve gauge invariance, we calculate one-loop corrections to the tree-level cross section. Because gauge invariance is preserved order-by-order in perturbation theory, the resulting theory will certainly be gauge invariant. At one loop, we have 13 diagrams we must evaluate, plus six counterterms. We show these diagrams below in Fig. 6.

Explicit expressions for these diagrams are given in Appendix B. Because we are calculating this model at one loop order, divergences appear which we must absorb into the definitions of our couplings and masses. We use the on-shell renormalization scheme:

$$\Sigma(p^2)\big|_{p^2=m^2} = 0, \quad (33)$$

$$\frac{d}{dp^2}\Sigma(p^2)\bigg|_{p^2=m^2} = 0, \quad (34)$$

$$\lim_{q\to 0}(-ie)\Gamma^\mu(p, p') = (-ie)2p^\mu. \quad (35)$$

Amaldi, Fubini, and Furlan in Ref. [21] provided the details of the relationship between the hadronic matrix element and the differential cross section, decomposed in terms of the longitudinal, transverse, and interference terms. We use the Mathematica package FEYNCALC [22,23] to determine our final expression for these structure functions, and then perform the loop integrals using QCDLOOP [24].

Form factors in the toy model

As a first check, we can examine the form factors generated by the loop corrections in this model. The nucleon form factor in this model is explicitly calculated in Appendix C. As one might predict, the corrections to the form factors generated by the inclusion of the loop diagrams are quite small. Because we are requiring the one-loop diagrams to contribute *all* the Q^2 behavior, this is problematic. To rectify this, we have chosen to change the coupling which controls the strength of the loop

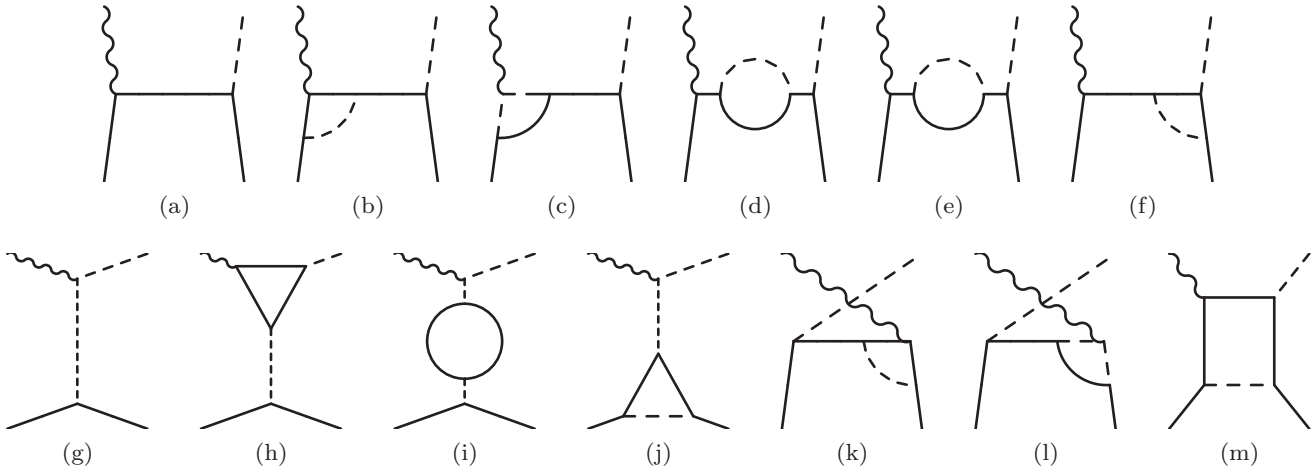

FIG. 6. Diagrams contributing to $\gamma^* + p \to \pi + n$. We list first all s-channel diagrams, all t-channel diagrams, both u-channel diagrams, and the single box diagram. Explicit equations are given for each of the 13 diagrams shown here.

corrections, as well as the masses of the particles propagating in the loops. In other words, we take $m_N \to m'_N$, $m_\pi \to m'_\pi$, and $g_{\pi N} \to g'_{\pi N}$ in the loop integrals only.

Clearly from the point of view of a consistent quantum field theoretic calculation, this approach is incorrect. Note, however, that because we do this consistently to each loop diagram, we preserve gauge invariance in this approach. As we are interested in the toy model only from the point of view of determining how well one may extract the pion form factor, rather than attempting to produce a fully consistent calculation, we believe the results are qualitatively meaningful.

Our chosen parameters are given in Table I. We select parameters to ensure a reasonable separation between F_p and F_π and also so that F_π falls off slower than F_p, as occurs in nature. Because we wish to describe the pion form factor with a monopole form factor, it is important to check that this is a good approximation. We find that the model form factor is well described for a monopole mass parameter of $\Lambda_\pi^2 = 5.56\,\mathrm{GeV}^2$. This fit is shown in Fig. 7.

With the free parameters in our model chosen, we may proceed to calculate the cross section and attempt to extract the model pion form factor.

VII. EXTRACTION OF THE PION FORM FACTOR

The F_π Collaboration reports the pion electromagnetic form factor for eight kinematic points, so in our first analysis, we attempt to extract those same points (see Table II). We follow a simplified version of their analysis outlined above in Sec. III C. We outline the steps of the analysis here.

(1) We calculate the loop corrected cross section, with the form factors described in the previous section. This cross section is called *pseudodata* in the following step. The model pion form factor $F_\pi(Q^2)$ shown in Fig. 7 is extracted from this cross section.

(2) We generate pseudodata for a range of t values for fixed Q^2 and W (dashed green line in Fig. 8). As with the F_π Collaboration, we choose the range of t to start near the minimum allowed value for the chosen kinematics. Specifically, the cross section is calculated between the minimum and maximum values of t measured (see Ref. [11] for explicit values).

(3) We define our model to be the tree-level matrix element, and incorporate the pion form factor as a multiplicative factor to the amplitude. This mirrors the approach in the VGL model. Thus our matrix

TABLE I. Tree-level and loop parameters used in this study. All parameters are in units of GeV.

$g_{\pi N}$	m_N	m_π	$g'_{\pi N}$	m'_N	m'_π
1.4	0.94	0.14	20	0.7	0.71

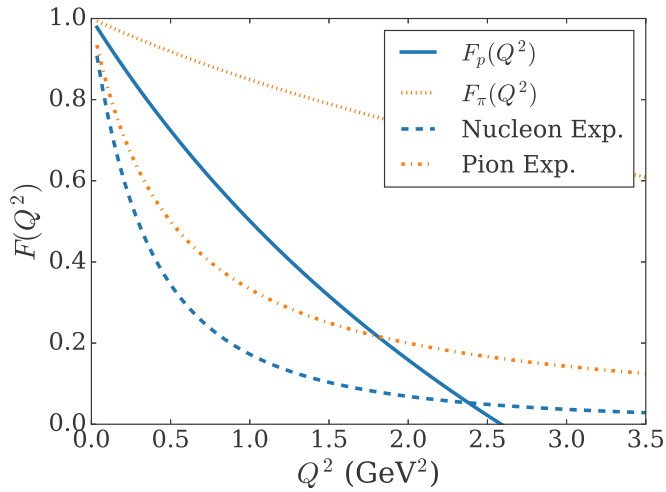

FIG. 7. Comparison of predicted electromagnetic pion (short dashed curve) and nucleon (solid curve) form factors with parametrizations of the pion (dot-dashed curve) and nucleon (dashed curve) form factors from data. In principal, there is also a neutron form factor, but because of the chosen mass parameters ($m'_N \approx m'_\pi$), the neutron form factor is approximately zero (see Appendix B for details). With a monopole mass of $\Lambda_\pi^2 = 5.56\,\mathrm{GeV}^2$, the toy model form factor may be replicated with a monopole form factor.

TABLE II. The F_π Collaboration extracted the pion electromagnetic form factor at eight kinematic points. We extract the same eight kinematic points.

Q^2 (GeV^2)	W (GeV)	$\lvert t_{\rm low}\rvert$ (GeV^2)	$\lvert t_{\rm high}\rvert$ (GeV^2)
0.35	2.10	0.010	0.040
0.60	1.95	0.025	0.074
0.70	2.19	0.030	0.250
0.75	1.95	0.037	0.093
1.00	1.95	0.060	0.140
1.60	1.95	0.135	0.255
1.60	2.22	0.079	0.215
2.45	2.22	0.145	0.365

element is

$$i\mathcal{M}^\mu = i\mathcal{M}^\mu_{\rm BTM} F_\pi(Q^2). \tag{36}$$

(4) We fit our model to the pseudodata to obtain our best fit for the parameter Λ_π^2. This value of Λ_π^2 corresponds to the extracted pion form factor (solid blue line in Fig. 8).
(5) We plot the resulting extracted pion form factors (see Figs. 9 and 10).

See Table III for a comparison of our analysis to the original F_π analysis

VIII. DISCUSSION OF THE RESULTS

Examining the fitted model cross sections shown in Figs. 14, 15, we can see that the agreement of the fitted model cross section when compared with pseudodata decreases slightly as we go to larger Q^2. We note, however, that with the exception of the $(Q^2, W) = (1.6, 1.95)$ and (2.45,2.22) kinematics, the disagreement between the model and pseudodata is less than 10 percent (see Fig. 10). Given the current experimental uncertainties are of this order, we conclude that the VGL model

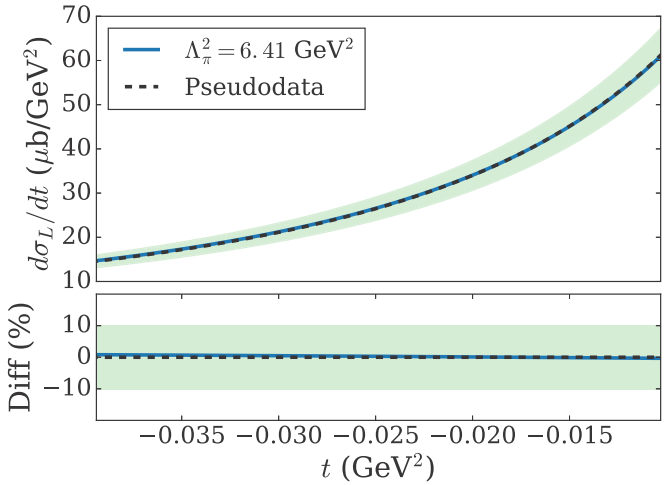

FIG. 8. Fitting simplified model of cross section to model cross section. Both the pseudodata (dashed black curve) and simplified model (solid blue curve) sit over one another. The extracted Λ_π^2 is related to the extracted pion from factor via $F_\pi(Q^2) = (1 + Q^2/\Lambda_\pi^2)^{-1}$.

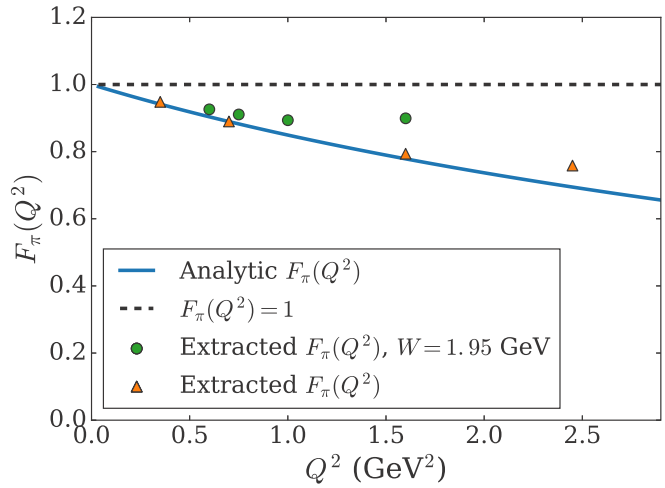

FIG. 9. Extracted F_π in our toy model, compared with true model form factor.

implementation of gauge invariance should model the cross section reasonably well over the kinematic range examined. This conclusion is borne out by the experimental data in Ref [8].

At low momentum transfer, we find that our extracted form factor is in good agreement with the true form factor in the toy model, although in general, we find a better agreement for data points extracted at larger W. As the momentum transfer increases, our extracted form factor tends to become a slightly worse representation of the true form factor. In particular, we note from Fig. 11, that the extracted form factor appears to trend away from the true form factor.

As noted in Ref. [11], the smallest kinematically allowed absolute value of t, denoted $|t_{\rm min}|$ may be reduced by measuring at larger W, or at smaller Q^2. This is important, as this reduces the distance that one has to extrapolate to reach the pion pole. In other words, for smaller absolute value of t, the

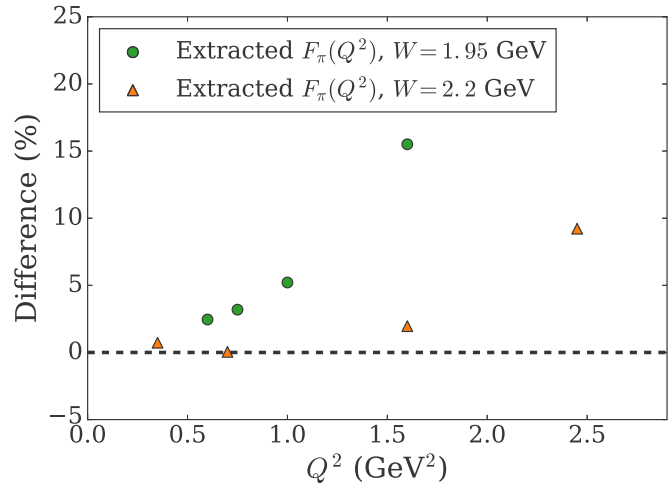

FIG. 10. Percentage difference between our extracted form factor and the true model form factor. Note that a positive difference corresponds to an overestimation of F_π. Thus for the kinematic points surveyed, the extracted form factor is overestimated.

TABLE III. Comparison of our analysis with the F_π Collaboration analysis. We calculate the cross section for this process in a simple model, and attempt to extract the pion form factor using a simple "VGL-like" model. Because of the model's simplicity, we may also calculate the pion form factor directly. The comparison of the extracted and calculated form factors allows one to study the possible model dependence of the extracted pion form factor.

	This analysis	F_π Collaboration
Model	$i\mathcal{M}^{\mu}_{\text{VGL-like}}$	$i\mathcal{M}^{\mu}_{\text{VGL}}$
	$\downarrow$ fit to …$\downarrow$	$\downarrow$ fit to …$\downarrow$
Data	$i\mathcal{M}^{\mu}_{\text{1-Loop}}$	$^1\text{H}(e, e'\pi^+)n$

pion photon interaction which occurs in the t channel looks more like the pion electromagnetic form factor measured in elastic $e^- + \pi^+$ scattering.

To verify our explanation, we extracted the model form factor at $W = 1.95\,\text{GeV}$ and $W = 2.2\,\text{GeV}$, for a range of Q^2 between 0 and $3\,\text{GeV}^2$, using the method outline above. The experimental data approximately spans the first 5% of the allowed t range. We therefore attempt to fit our model cross section to the pseudodata over the first 5% of the allowed t kinematic range for the chosen Q^2 and W.

The results of this process are shown in Fig. 11. As predicted, the agreement between the extracted form factor and the model form factor are good for a larger range of Q^2 when the $W = 2.2\,\text{GeV}$ data is used. This data clearly shows the way the model form factor is being systematically overestimated for increasing Q^2.

It is interesting to speculate about the way this result could carry over to the extraction of the real pion form factor from real data. Indeed, if the relation between the extracted and true pion form factor remained quantitatively the same, this would suggest (experimental uncertainties notwithstanding) that the extracted pion form factor values are currently overestimated. This effect—if observed—would imply that the "true" pion form factor was smaller, bringing the extracted pion form factor closer to the asymptotic limit predicted by perturbative QCD.

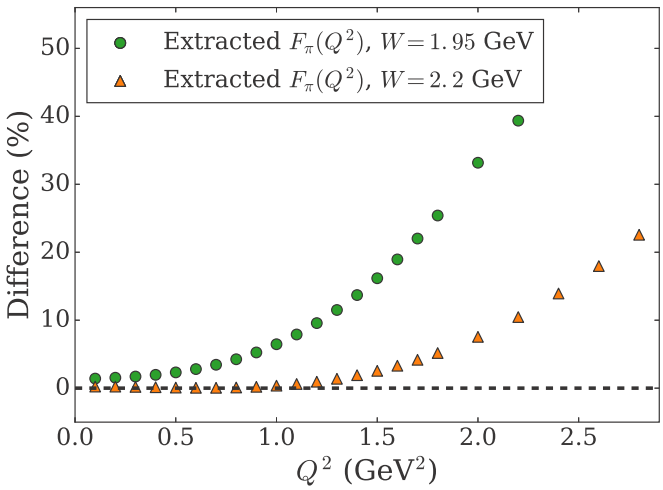

FIG. 11. Extracting the pion form factor near the minimum kinematically allowed t value. Note that the agreement between the true form factor and the extracted form factor worsens sooner for the $W = 1.95\,\text{GeV}$ data, because $|t_{\text{min}}|$ is larger. Thus the pion photon interaction looks less like the on-shell pion electromagnetic form factor.

IX. CONCLUSION

We began by discussing the theoretical drawbacks with the implementation of gauge invariance in the VGL model. In particular, we discussed the unnatural factorization of the pion form factor from the matrix element. We proposed a simple toy model which we used to generate pseudodata for pion electroproduction. We followed the F_π Collaboration's approach to extract the toy model's pion form factor. The extracted pion form factor was compared to the true form factor, and it was found that our extracted form factor was in all cases *larger* than the true form factor. If this result were to hold in the extraction of the experimental pion form factor, it would suggest that the extracted pion form factor is currently overestimated.

Although the present work was simplified by using only bosonic fields, we believe that the results may provide guidance concerning the role of a full implementation of gauge invariance in the physical system. The extension of the present work to the case of fermions is clearly a high priority.

ACKNOWLEDGMENTS

We thank R. Young, G. Miller, and J. Zanotti for helpful discussions. This work was supported by the University of Adelaide and by the Australian Research Council through the ARC Centre of Excellence for Particle Physics at the Terascale (Grant No. CE110001104) and Discovery Projects No. DP150103101 and No. DP180100497.

APPENDIX A: SCALAR AND VECTOR LOOP INTEGRALS

We define the following loop integrals. q_i are the external particle momenta, all understood to be entering the diagram. Thus conservation of momentum is $q_1 + q_2 + q_3 + q_4 = 0$. In the case of the vector three- and four-point functions, we note that the sign of the external momentum is important.

1. Scalar two-point function:

$$B_0\left(q_1^2; m_1^2, m_2^2\right) = \int \frac{d^4k}{(2\pi)^4} \frac{1}{\left[k^2 - m_1^2 + i\epsilon\right]} \times \frac{1}{\left[(k+q_1)^2 - m_2^2 + i\epsilon\right]}. \tag{A1}$$

2. Scalar three-point function:

$$C_0\left(q_1^2, q_2^2, q_3^2; m_1^2, m_2^2, m_3^2\right) = \int \frac{d^4k}{(2\pi)^4} \frac{1}{\left[k^2 - m_1^2 + i\epsilon\right]} \frac{1}{\left[(k+q_1)^2 - m_2^2 + i\epsilon\right]} \times \frac{1}{\left[(k+q_1+q_2)^2 - m_3^2 + i\epsilon\right]}. \tag{A2}$$

3. Scalar four-point function:

$$D_0\big(q_1^2, q_2^2, q_3^2, q_4^2, (q_1+q_2)^2, (q_1+q_4)^2, m_1^2, m_2^2, m_3^2, m_4^2\big) = \int \frac{d^4k}{(2\pi)^4} \frac{1}{\big[k^2 - m_1^2 + i\epsilon\big]} \frac{1}{\big[(k+q_1)^2 - m_2^2 + i\epsilon\big]} \times \frac{1}{\big[(k+q_1+q_2)^2 - m_3^2 + i\epsilon\big]} \times \frac{1}{\big[(k+q_1+q_2+q_3)^2 - m_4^2 + i\epsilon\big]}. \tag{A3}$$

4. Vector three-point function:

$$C_1^\mu\big(q_1, q_2, q_3; m_1^2, m_2^2, m_3^2\big) = \int \frac{d^4k}{(2\pi)^4} \frac{1}{\big[k^2 - m_1^2 + i\epsilon\big]} \frac{(2q_1+q_2+2k)^\mu}{\big[(k+q_1)^2 - m_2^2 + i\epsilon\big]} \times \frac{1}{\big[(k+q_1+q_2)^2 - m_3^2 + i\epsilon\big]}. \tag{A4}$$

5. Vector four-point function:

$$D_1^\mu\big(q_1, q_2, q_3, q_4, m_1^2, m_2^2, m_3^2, m_4^2\big) = \int \frac{d^4k}{(2\pi)^4} \frac{1}{\big[k^2 - m_1^2 + i\epsilon\big]} \frac{(2q_1+q_2+2k)^\mu}{\big[(k+q_1)^2 - m_2^2 + i\epsilon\big]} \times \frac{1}{\big[(k+q_1+q_2)^2 - m_3^2 + i\epsilon\big]} \times \frac{1}{\big[(k+q_1+q_2+q_3)^2 - m_4^2 + i\epsilon\big]}. \tag{A5}$$

Making use of these definitions, we may write the loop correction expressions.

APPENDIX B: EVALUATION OF DIAGRAMS

We begin with the two tree-level diagrams. The s-channel diagram is

$$i\mathcal{M}^{(a)\mu} = (-i\sqrt{2}g_{\pi N}) S_F^N(p_s)(-ie)(p+p_s)^\mu. \tag{B1}$$

The t-channel diagram is

$$i\mathcal{M}^{(g)\mu} = (-i\sqrt{2}g_{\pi N}) S_F^\pi(p_t)(-ie)(p_t+p_\pi)^\mu. \tag{B2}$$

The two s-channel vertex corrections are

$$i\mathcal{M}^{(b)\mu} = (-i\sqrt{2}g_{\pi N}) S_F^N(p_s) \times (-ie)\big[ig'^2_{\pi N} C_1^\mu\big(p, q, -p_s; m'^2_\pi, m'^2_N, m'^2_N\big)\big], \tag{B3}$$

$$i\mathcal{M}^{(c)\mu} = (-i\sqrt{2}g_{\pi N}) S_F^N(p_s) \times (-ie)\big[2ig'^2_{\pi N} C_1^\mu\big(p, q, -p_s; m'^2_N m'^2_\pi, m'^2_\pi\big)\big]. \tag{B4}$$

There are two self-energy diagrams, corresponding to a virtual charged and neutral pion, respectively:

$$i\mathcal{M}^{(d)\mu} = (-i\sqrt{2}g_{\pi N}) S_F^N(p_s)\big[2g'^2_{\pi N} B_0\big(p_s^2, m'^2_N, m'^2_\pi\big)\big] \times S_F^N(p_s)(-ie)(p+p_s)^\mu, \tag{B5}$$

$$i\mathcal{M}^{(e)\mu} = (-i\sqrt{2}g_{\pi N}) S_F^N(p_s)\big[g'^2_{\pi N} B_0\big(p_s^2, m'^2_N, m'^2_\pi\big)\big] \times S_F^N(p_s)(-ie)(p+p_s)^\mu. \tag{B6}$$

The strong vertex is also modified by the loop corrections:

$$i\mathcal{M}^{(f)\mu} = (-i\sqrt{2}g_{\pi N})\big[ig'^2_{\pi N} C_0\big(p_s^2, p_\pi^2, p'^2, m'^2_\pi, m'^2_N, m'^2_N\big)\big] \times S_F^N(p_s)(-ie)(p+p_s)^\mu. \tag{B7}$$

There is one diagram which modifies the pion electromagnetic vertex:

$$i\mathcal{M}^{(h)\mu} = (-i\sqrt{2}g_{\pi N}) S_F^\pi(p_t) \times (-ie)\big[2ig'^2_{\pi N} C_1^\mu\big(p_t, q, -p_\pi, m'^2_N, m'^2_N, m'^2_N\big)\big], \tag{B8}$$

and one self-energy diagram:

$$i\mathcal{M}^{(i)\mu} = (-i\sqrt{2}g_{\pi N}) S_F^\pi(p_t)\big[2g'^2_{\pi N} B_0\big(p_t^2, m'^2_N, m'^2_N\big)\big] \times S_F^\pi(p_t)(-ie)(p_t+p_\pi)^\mu. \tag{B9}$$

The t-channel strong vertex is also modified:

$$i\mathcal{M}^{(j)\mu} = (-i\sqrt{2}g_{\pi N})\big[ig'^2_{\pi N} C_0\big(p^2, p_t^2, p'^2, m'^2_\pi, m'^2_N, m'^2_N\big)\big] \times S_F^\pi(p_t)(-ie)(p_t+p_\pi)^\mu. \tag{B10}$$

At tree level, there are no u-channel diagrams, because the neutron is neutral. However, quantum corrections modify the tree-level result. There are two corrections to the electromagnetic vertex:

$$i\mathcal{M}^{(k)\mu} = (-ie)\big[2ig'^2_{\pi N} C_1^\mu\big(p_u, q, -p'; m'^2_\pi, m'^2_N, m'^2_N\big)\big] \times S_F^N(p_u)(-i\sqrt{2}g_{\pi N}), \tag{B11}$$

$$i\mathcal{M}^{(l)\mu} = (+ie)\big[2ig'^2_{\pi N} C_1^\mu\big(p_u, q, -p'; m'^2_N, m'^2_\pi, m'^2_\pi\big)\big] \times S_F^N(p_u)(-i\sqrt{2}g_{\pi N}). \tag{B12}$$

Note that these come in with the opposite sign. Because we choose $m'_\pi = 0.7\,\text{GeV}$ and $m'_N = 0.71\,\text{GeV}$, these two terms

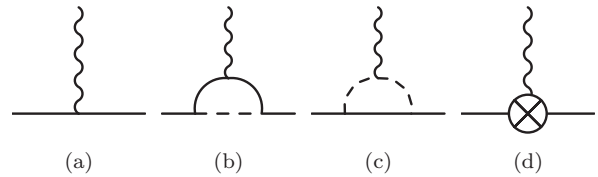

FIG. 12. Diagrams which contribute to the calculation of the electromagnetic form factor of the proton.

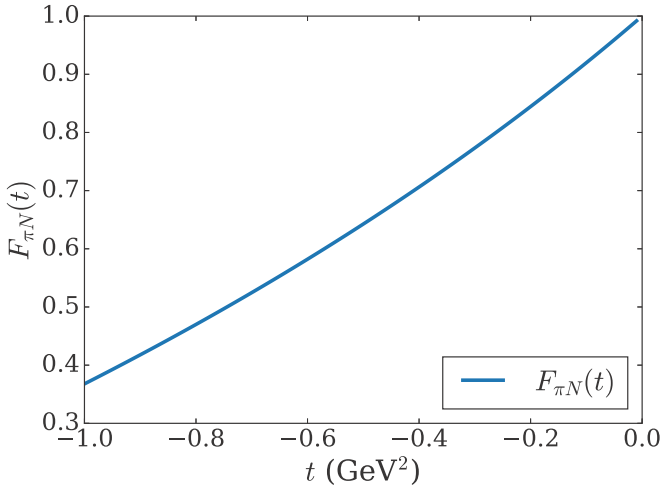

FIG. 13. Strong form factor predicted in toy model. Note that because we evaluate the cross section for small $|t|$, the main source of t dependence in the cross section comes from the t-channel propagator.

have approximately the same magnitude, but opposite sign. Thus the neutron's effect on the cross section is negligible. The single box diagram is

$$i\mathcal{M}^{(m)\mu} = (-i\sqrt{2}g_{\pi N})(-ie) \times \left[-g'^2_{\pi N} D_1^{\mu}\left(p, q, -p_\pi, -p', m'^2_\pi, m'^2_N, m'^2_N, m'^2_N\right)\right]. \tag{B13}$$

APPENDIX C: CALCULATING ELECTROMAGNETIC FORM FACTORS IN THE TOY MODEL

For completeness we demonstrate how the calculation for the electromagnetic vertex proceeds. The diagrams which contribute to the proton electromagnetic vertex are shown in Fig. 12. We may summarize this result algebraically as

$$\Gamma_N^{\mu}(p, p'; q) = \Gamma_{N,a}^{\mu}(p, p'; q) + \Gamma_{N,b}^{\mu}(p, p'; q) + \Gamma_{N,c}^{\mu}(p, p'; q) + \Gamma_{N,\text{c.t.}}^{\mu}(p, p'; q), \tag{C1}$$

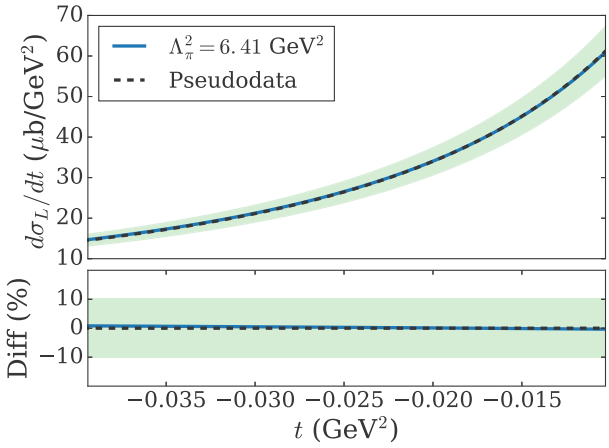

(a) $Q^2 = 0.35$ GeV^2, $W = 2.10$ GeV

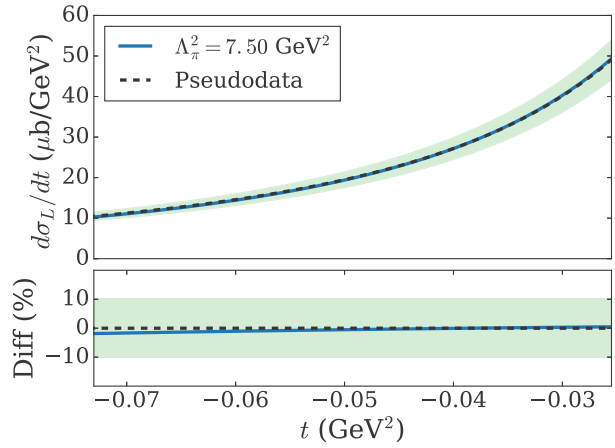

(b) $Q^2 = 0.60$ GeV^2, $W = 1.95$ GeV

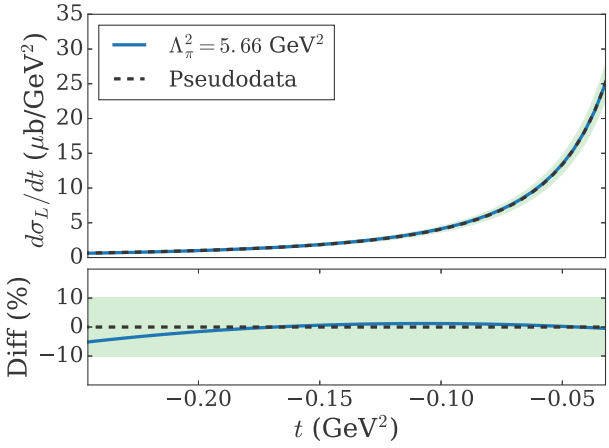

(c) $Q^2 = 0.70$ GeV^2, $W = 2.19$ GeV

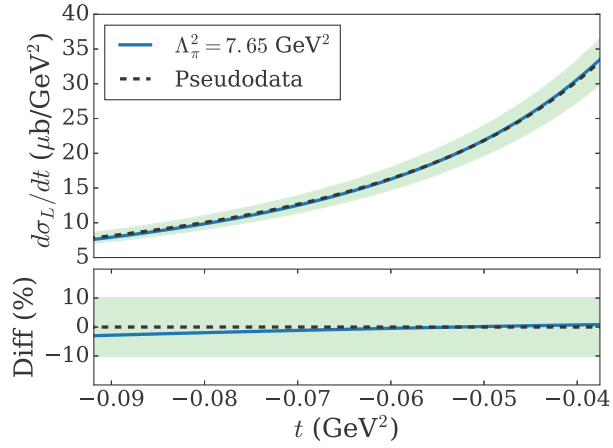

(d) $Q^2 = 0.75$ GeV^2, $W = 1.95$ GeV

FIG. 14. Fitting simplified model of cross section to pseudodata. Both the pseudodata (dashed black) and simplified model (solid blue) sit over one another. The extracted Λ_π^2 is related to the extracted pion from factor via $F_\pi(Q^2) = (1 + Q^2/\Lambda_\pi^2)^{-1}$.

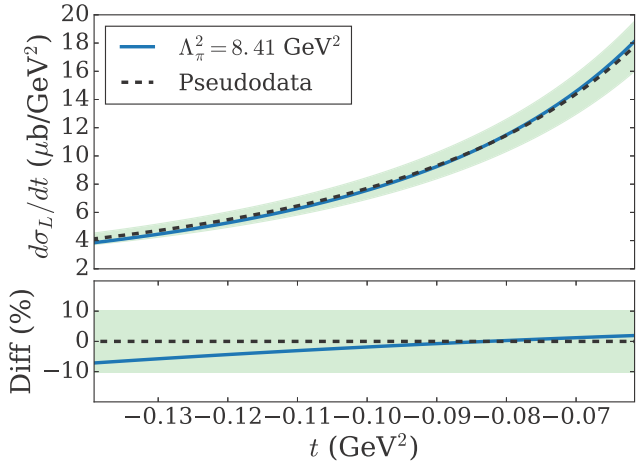

(a) $Q^2 = 1.00$ GeV^2, $W = 1.95$ GeV

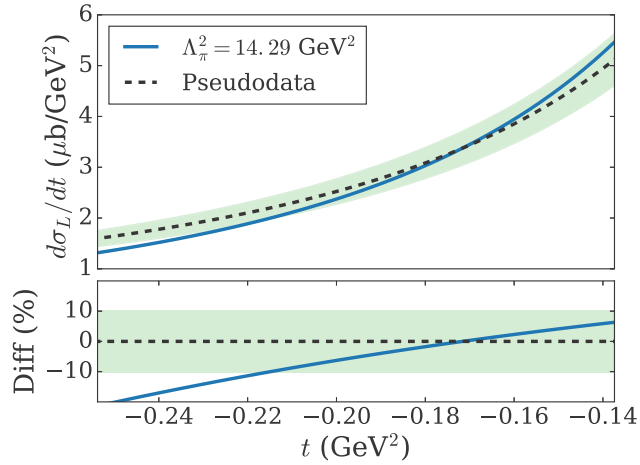

(b) $Q^2 = 1.60$ GeV^2, $W = 1.95$ GeV

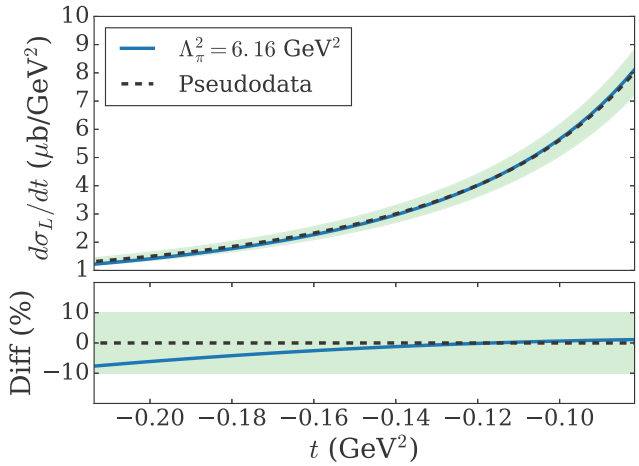

(c) $Q^2 = 1.60$ GeV^2, $W = 2.22$ GeV

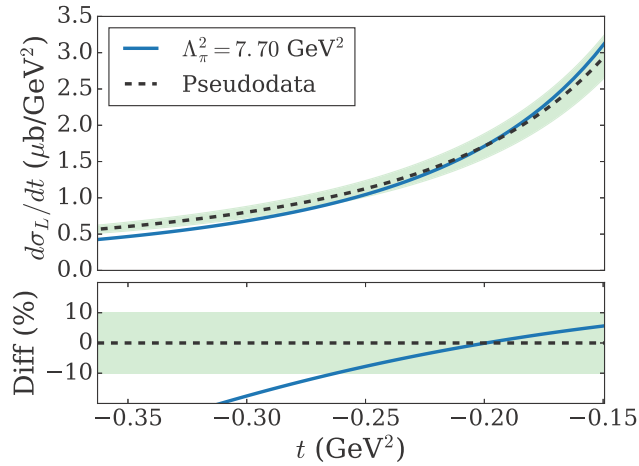

(d) $Q^2 = 2.45$ GeV^2, $W = 2.22$ GeV

FIG. 15. Similar to Fig. 14, fitting simplified model of cross section to pseudodata. Both the pseudodata (dashed black) and simplified model (solid blue) sit over one another. The extracted Λ_π^2 is related to the extracted pion from factor via $F_\pi(Q^2) = (1 + Q^2/\Lambda_\pi^2)^{-1}$.

where $q = p' - p$. Using the Feynman Rules we may write down each contribution as

$$\Gamma^\mu_{N,a}(p, p'; q) = (p + p')^\mu, \tag{C2}$$

$$\Gamma^\mu_{N,b}(p, p'; q) = ig'^2_{\pi N} C_1^\mu\big(p, q, p'; m'^2_\pi, m'^2_N, m'^2_N\big), \tag{C3}$$

$$\Gamma^\mu_{N,c}(p, p'; q) = 2ig'^2_{\pi N} C_1^\mu\big(p, q, p'; m'^2_N, m'^2_\pi, m'^2_\pi\big), \tag{C4}$$

$$\Gamma^\mu_{N,\text{c.t.}}(p, p'; q) = (p + p')^\mu \delta_e. \tag{C5}$$

We use the on-shell renormalization scheme. This requires that

$$\lim_{q\to 0} \Gamma^\mu_N(p, p'; q) = (2p)^\mu. \tag{C6}$$

It is possible to show that

$$\lim_{q\to 0} C_1^\mu\big(p_1, p_2, m_1^2, m_2^2, m_2^2\big) = -2p_1^\mu \frac{d}{dp_1^2} B_0\big(p_1, m_1^2, m_2^2\big). \tag{C7}$$

Thus its possible to show that the counterterm is

$$\delta_e = 3ig'^2_{\pi N} \frac{d}{dp^2} B_0\big(p, m'^2_N, m'^2_2\big)\big|_{p^2 = m'^2_N}. \tag{C8}$$

APPENDIX D: FITTED CROSS SECTIONS

The F_π Collaboration reported extracted pion form factor values for eight kinematic points. In our first analysis, we extracted the same kinematic points in our model. This required us to fit out model cross section to the pseudodata calculated using the loop-corrected cross section for each of the eight kinematic sets (see Table II). The following eight plots show the agreement between the pseudodata, and our model cross section. In each case, the extracted pion form factor shown in Fig. 9 is obtained by evaluating the monopole form factor using the best fit for the monopole mass Λ_π^2.

We also include the calculated "strong" (πN) form factor which one encounters in the t-channel process.

[1] G. A. Miller, Ann. Rev. Nucl. Part. Sci. **60**, 1 (2010).
[2] A. J. Chambers, J. Dragos, R. Horsley, Y. Nakamura, H. Perlt, D. Pleiter, P. E. L. Rakow, G. Schierholz, A. Schiller, K. Somfleth, H. Stuben, R. D. Young, and J. M. Zanotti, Phys. Rev. D **96**, 114509 (2017).
[3] I. C. Cloet, W. Bentz, and A. W. Thomas, Phys. Rev. C **90**, 045202 (2014).
[4] P. Maris and P. C. Tandy, Phys. Rev. C **62**, 055204 (2000).
[5] G. P. Lepage and S. J. Brodsky, Phys. Lett. **87B**, 359 (1979).
[6] L. Chang, I. C. Cloet, C. D. Roberts, S. M. Schmidt, and P. C. Tandy, Phys. Rev. Lett. **111**, 141802 (2013).
[7] S. R. Amendolia *et al.* (NA7 Collaboration), Nucl. Phys. B **277**, 168 (1986).
[8] G. M. Huber *et al.* (The Jefferson Lab F_π Collaboration), Phys. Rev. C **78**, 045203 (2008).
[9] S.-X. Qin, C. Chen, C. Mezrag, and C. D. Roberts, Phys. Rev. C **97**, 015203 (2018).
[10] S. Galster, H. Klein, J. Moritz, K. H. Schmidt, D. Wegener, and J. Bleckwenn, Nucl. Phys. B **32**, 221 (1971).
[11] H. P. Blok *et al.* (Jefferson Lab F_π Collaboration), Phys. Rev. C **78**, 045202 (2008).
[12] M. M. Kaskulov, K. Gallmeister, and U. Mosel, Phys. Rev. D **78**, 114022 (2008).
[13] M. Vanderhaeghen, M. Guidal, and J. M. Laget, Phys. Rev. C **57**, 1454 (1998).
[14] M. Guidal, J. M. Laget, and M. Vanderhaeghen, Phys. Lett. B **400**, 6 (1997).
[15] C.-R. Ji, W. Melnitchouk, and A. W. Thomas, Phys. Rev. D **88**, 076005 (2013).
[16] J. C. Ward, Phys. Rev. **78**, 182 (1950).
[17] H. S. Green, Phys. Rev. **95**, 548 (1954).
[18] Y. Takahashi, Nuovo Cim. **6**, 371 (1957).
[19] K. Nishijima, Physical Review **122**, 298 (1961).
[20] G. A. Miller, Phys. Rev. C **80**, 045210 (2009).
[21] E. Amaldi, S. Fubini, and G. Furlan, Springer Tracts Mod. Phys. **83**, 1 (1979).
[22] R. Mertig, M. Bohm, and A. Denner, Comput. Phys. Commun. **64**, 345 (1991).
[23] V. Shtabovenko, R. Mertig, and F. Orellana, Comput. Phys. Commun. **207**, 432 (2016).
[24] R. K. Ellis and G. Zanderighi, J. High Energy Phys. 02 (2008) 002.